

PAPER

# Observation of self-polarization in BSA protected Au<sub>20</sub> clusters

To cite this article: D K Swain *et al* 2017 *Nanotechnology* **28** 445704

View the [article online](#) for updates and enhancements.

# Observation of self-polarization in BSA protected Au<sub>20</sub> clusters

D K Swain<sup>1</sup>, A Narzary<sup>1</sup>, A K Singh<sup>2</sup> , A Chandra<sup>3</sup>, T Nagasawa<sup>4</sup>, S Yamamoto<sup>4</sup>, M Mitsuishi<sup>4</sup> and S Rath<sup>1</sup>

<sup>1</sup>School of Basic Sciences, Indian Institute of Technology Bhubaneswar, Jatni, 752050, Odisha, India

<sup>2</sup>Department of Physics and Astronomy, National Institute of Technology, Rourkela, 769008, Odisha, India

<sup>3</sup>Department of Physics, Indian Institute of Technology, Kharagpur-721 302, India

<sup>4</sup>Institute of Multidisciplinary Research for Advanced Materials, Tohoku University, 2-1-1 Katahira, Aoba-Ku, Sendai 980-8577, Japan

E-mail: [srath@iitbbs.ac.in](mailto:srath@iitbbs.ac.in)

Received 4 June 2017, revised 12 August 2017

Accepted for publication 18 August 2017

Published 5 October 2017



CrossMark

## Abstract

Bovine serum albumin (BSA)-protected gold clusters (atomicity  $\sim 20$ ), prepared using a wet chemical route, show strong dipolar radiative transition with a gap energy of 1.93 eV due to the high oscillator strength, as confirmed by the emission studies. Self-arrangement of the clusters with fixed atomicity yields a low dispersive dielectric and electric self-polarization nature. The electrical hysteresis loop measurements returned a remanent polarization of  $0.05 \mu\text{C cm}^{-2}$ , which can be correlated with the dipolar orientation (activation energy  $\sim 45.32 \text{ meV}$ ), originating from the structure-dependent deformation of the charge density.

Keywords: gold cluster, optical properties, dielectric properties, electric polarization

(Some figures may appear in colour only in the online journal)

## 1. Introduction

Optical- and/or electrical-field-mediated polarization in nano-materials and clusters is an intriguing phenomenon for a myriad of applications, including self-powered electronic systems [1], energy harvesting [2], molecular switches [3], memory devices [4], sensors [5] etc. Polarization and electronic effects in nanoparticles with a high degree of confinement (e.g. atomic clusters) are predominantly governed by atomicity and symmetry [6, 7]. Metal clusters of niobium ( $\text{Nb}_n$ ), rhodium ( $\text{Rd}_n$ ) and gold ( $\text{Au}_n$ ) have been found to exhibit strong electric polarization. The results are attributed to the anisotropic structure of small clusters (atomicity  $< 15$ ) and/or the hollow cage structure in medium-sized clusters (atomicity  $> 35$ ) [8–10]. To date, polarization in hetero-nuclear clusters is understood in terms of the charge transfer between unlike atoms. However, the origin of spontaneous electric dipoles in homo-nuclear metal clusters is rather obscure. There are only a few recent theoretical studies that have correlated the observed electronic properties with the intrinsic moment, which originates due to the presence

of the symmetry-broken states below the critical temperature [11] and the domination of directional bonding in the structural anisotropy [12].

More recently, the gold clusters with a size in the range of 2 nm, have been found to exhibit exciting properties, namely (1) the size-dependent opening of the electronic band gap between the electronic states, (2) a reduction of non-radiative relaxation and (3) the enhancement of the radiative process. This leads to the observation of strong emission properties with a high oscillator strength [13]. According to the theory and experimental observation [14],  $\text{Au}_{20}$  is considered to be a highly stable cluster exhibiting a distinct energy gap of 1.77 eV between the highest occupied molecular orbital (HOMO) and the lowest unoccupied molecular orbital (LUMO). A time-dependent optical study based on density functional theory also indicates strong optical non-linearity controlled by dipole polarizability, due to the preferred atomic site-specific charge transfer in the  $\text{Au}_n$  clusters [15]. Regardless of the theoretical progress, experimental proof for the appearance of the electric dipole moment and

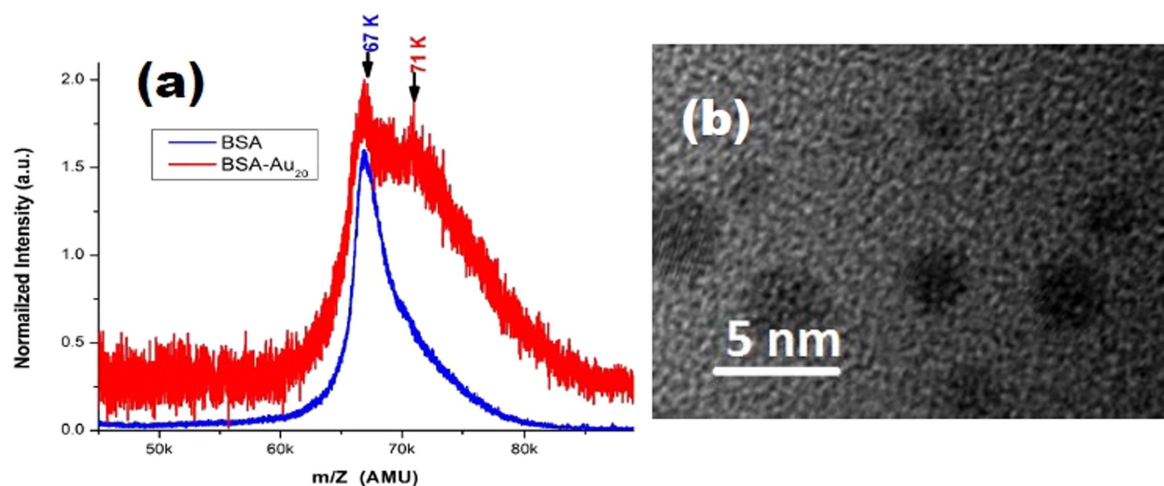


**Figure 1.** (a) The MALDI-TOF mass spectra of the BSA-Au<sub>20</sub> (red) and BSA (blue); (b) a TEM micrograph of the BSA-Au<sub>20</sub> taken at an acceleration voltage of 300 kV.

polarizability in the homo-nuclear atomic clusters remains elusive.

In this paper, we present conclusive evidence to show that Au<sub>20</sub> metal clusters (MCs) grown through biomolecule mediation exhibit electric dipole moments, which can be reversibly polarized as a function of the applied ac signal. The behavior is quite similar to that observed in ferroelectric materials, and therefore shows appreciable temperature-dependent modulation of the physical properties such as dielectric and electric polarization, etc.

## 2. Experimental methods

Atomic gold clusters with an atomicity of 20 (Au<sub>20</sub>) were synthesized by controlling the interactions of the functionalized biomolecules. In a typical synthesis process, an aqueous solution of gold chloride tetrahydrate (HAuCl<sub>4</sub>, 10 ml, 10 mM) was allowed to interact with a bovine serum albumin aqueous solution (BSA, 10 ml, 50 mg ml<sup>-1</sup>). After the mixed solution was homogenized under vigorous stirring for 30 min, sodium hydroxide solution (NaOH, 1 ml, 1 M) was added to the above solution. To ensure the reduction process was complete, the solution was left to be stirred at a temperature of 30 °C for 12 h. Subsequently, the color of the solution gradually changed from light yellow to deep brown. The Au<sub>20</sub> MC powders were collected by repeatedly washing them with ethanol and double distilled water using a centrifuge. Then, the samples were characterized using matrix-assisted laser desorption time-of-flight (MALDI-TOF) mass spectroscopy, transmission electron microscopy (TEM), emission spectroscopy, dielectric and electric polarization measurements.

## 3. Results and discussion

To estimate the atomicity of the samples, the MALDI-TOF mass spectrometry measurements were conducted using a

Bruker Reflex III Autoflex speed mass spectrometer equipped with a nitrogen laser (337 nm). An aqueous solution of 2,5-dihydroxybenzoic acid (DHB) matrix (10 mg ml<sup>-1</sup>) was mixed with sample solutions (5 mg ml<sup>-1</sup>) with a mixing ratio of 5:1. A droplet of the solution was dropped onto a target plate (MTP 384 target plate ground steel TF (Bruker Daltonics)) and dried in a vacuum. The spectra were recorded in linear positive mode by accumulating the data from 3000 laser shots. Figure 1(a) shows the MALDI-TOF mass spectra of the pure BSA ligand and the BSA protected Au cluster (BSA-Au<sub>20</sub>) samples indicated by blue and red lines respectively. The mass spectra clearly indicate that the BSA has a mass of 67 kiloDalton (kDa). In comparison, the mass spectrum of the BSA-Au<sub>20</sub> contained two peaks, namely at 67 kDa and 71 kDa. Considering the mass difference between the two peaks, the peak at 71 kDa was assigned to BSA-Au<sub>20</sub>. Further, the size of the BSA-Au<sub>20</sub> samples was analyzed using transmission electron microscopy TEM (FEI, TF30) operated at 300 kV equipped with a GATAN Orius CCD camera. For the TEM studies, the samples were collected on a carbon-coated copper grid. Figure 1(b) shows the TEM micrographs of the BSA-Au<sub>20</sub>. Detailed analysis reveals that the average size varies from 2 nm to 5 nm. The smallest sized (~2 nm) particle may be attributed to the size of the Au<sub>20</sub>, whereas the largest one may be an agglomerated state of the clusters and the BSA.

To understand the optical response of the sample, emission measurements have been carried out using a Horiba Scientific FluroMax-4 spectrofluorometer in the presence of an excitation wavelength of 480 nm from a xenon lamp with a line power of 0.057 mW cm<sup>-2</sup>. For the measurements, the cluster samples were diluted 200 times and dispersed in a water medium. Figure 2 shows the emission spectra of BSA-Au<sub>20</sub> and BSA indicated by the red line and the blue line respectively. In contrast to the BSA, the BSA-Au<sub>20</sub> exhibited a strong emission at a wavelength of 640 nm. From the emission spectra, the band gap of the sample was estimated to be 1.93 eV. This shows a blue shift of 0.16 eV in comparison with the gas phase Au<sub>20</sub> (band gap,  $E_g \sim 1.77$  eV) [14].

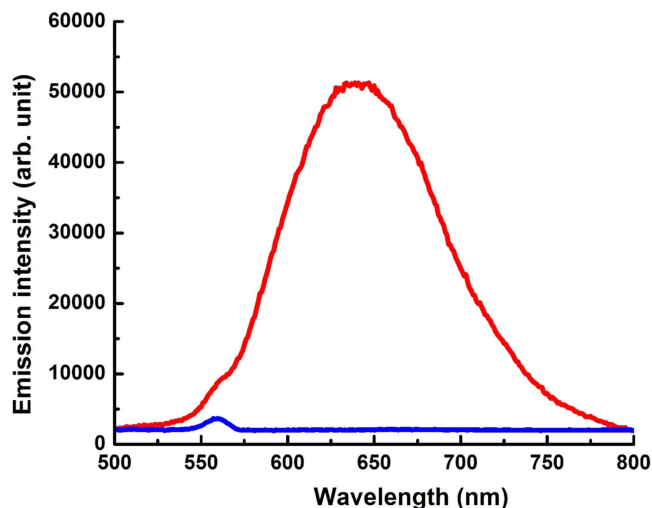


**Figure 2.** Emission spectra of the BSA-Au<sub>20</sub> (red line) and BSA (blue line).

Similarly, Jin *et al* [16] and Wang *et al* [17] observed a blue shift of 0.38 eV and 0.47 eV in the thiolate- and phosphine-protected Au<sub>20</sub> clusters respectively. From this analysis, the blue shift accomplished the role of ligand field effect on the electronic structure of Au<sub>20</sub> in addition to the strong confinement. Again, the intensity of the emission lines is dependent on [18] the transition probability of the excited states,  $T_r = \frac{\omega^4}{3\pi\epsilon_0 c^3} |M|^2$ , where  $\omega$ ,  $\epsilon_0$ ,  $c$ ,  $M$  are the frequency of the emission line, dielectric constant, the velocity of the light and the dipole moment matrix containing the excited and the ground states respectively. In addition to the extrinsic factors, namely the sample concentration and the intensity of the excitation light source, Jin *et al* [19] observed the enhancement of the emission intensity due to the increase in the electro-positivity of the metal (Au<sub>25</sub>) core, mediated by the charge transfer (from the ligand to the metal core). Raut *et al* [20] observed the strong polarization anisotropy from the BSA-protected Au<sub>25</sub> clusters due to the asymmetry of the electronic charge states involved in the transitions. Recently, Tian *et al* [21] affirmed the self-polarization-induced enhancement of the photoluminescence intensity of the ceramic powders. This indicates that the anisotropy in the charge distribution yields the enhancement of the emission intensity by increasing the dipole moment. The experimental reports by Wan *et al* [22] and Knoppe *et al* [23] suggest that Au<sub>20</sub> exhibits an inherent chirality and hyper-polarizability (a strong polarization effect in the presence of electromagnetic radiation) respectively. Therefore, the enhancement in emission intensity observed in our sample may be attributed to the increase in the dipole moment and oscillator strength of the excited state. However, a more systematic study is required to affirm the cause of the enhancement of the emission intensity.

The stabilization of ordered and reversible polar domains in a material can lead to its application in areas such as capacitors, sensors, actuators, etc [24]. To determine the feasibility of these applications, it is essential to determine the dielectric response as a function of temperature and

frequency. These measurements were carried out using a high-precision impedance analyzer (Wayne Kerr 6500B) over a frequency range of 0.1 kHz to 100 kHz. The temperature variation from 15 K–320 K was attained using a closed cycle refrigerator (Cryo industries, USA). For the dielectric measurements, the powder samples were made into a circular disc-like pellet (5 mm in diameter and 2 mm thick) with a silver coating on both the surfaces. Figure 3(a) shows the variation of the real part of the dielectric constant (RDEC) with the temperature at a given frequency. At a low frequency, the RDEC has a strong dielectric onset in the temperature range 200 K–300 K, while the onset shifts to a higher temperature upon increasing the frequency. Again, the RDEC varies linearly with temperature and is independent of the frequency in the temperature regime, 10 K–200 K. The sharp rise in the RDEC in the temperature range 200 K–300 K, may be due to the thermally activated local displacement of the electrons and the orientation of the dipole in the direction of the electric field. Further, as observed in figure 3(b), there is a continuous decrement of the RDEC in the frequency range 500–60 000 Hz for a given temperature condition varying from 200 K to 300 K. The frequency-dependent behavior of the RDEC spectrum was analyzed using the Debye relaxation relation  $\epsilon_r = \epsilon_\infty + \frac{(\epsilon_s - \epsilon_\infty)}{1 + \omega^2\tau^2}$  where  $\epsilon_s$ ,  $\epsilon_\infty$ ,  $\tau$  and  $\omega$  are the static dielectric permittivity, high frequency dielectric permittivity, relaxation time and frequency respectively. From the fitting using the above equation,  $\epsilon_s$  and  $\epsilon_\infty$  were estimated as  $3.15 \pm 0.02$  and  $3.46 \pm 0.03$  respectively at room temperature (300 K). The low dielectric relaxation strength ( $|\epsilon_s - \epsilon_\infty| = 0.31$ ) [25] can be attributed to the low dispersive nature of the sample. A similar dielectric constant has been observed in ultra-thin gold clusters by Nolte *et al* [26]. Abdelhalim *et al* [27] observed very strong dielectric dispersion from the Au nanoparticles with a size ranging from 10 to 50 nm. The inset of figure 3(b) shows the relaxation time  $\sim$  temperature plot. Using the Arrhenius ( $\tau = \tau_o e^{\frac{E_a}{k_b T}}$ ) type relaxation law, the activation energy,  $E_a$ , is estimated as 45.32 meV. The relaxation at a high temperature,  $\tau_o$ , is observed to be 3.6 ns. The attempt frequency of dipole orientation,  $f_o = \frac{1}{\tau_o}$ , becomes 0.27 GHz. This indicates that the permanent dipolar orientation was the dominant mechanism in the observed polarization, which was noted under the influence of the external electric field [28]. Further, the electric polarization (PE) properties of the BSA-Au<sub>20</sub> samples were studied using a Radiant Technology Inc. PE loop tracer with a frequency cycle of  $f = 500$  Hz and a temperature of 300 K in the presence of a poling field of  $4.5 \text{ kV cm}^{-1}$ . For the measurements, a sample pallet with a diameter of 5 mm and a thickness of 2 mm was prepared, and the electrodes were made by a silver bulk coating on both sides of the pallet. Figure 4(a) shows a hysteresis loop from the BSA-Au<sub>20</sub> samples. The coercive field,  $E_c = (E_{c+} - E_{c-})/2$  is estimated to be  $4.80 \text{ kV cm}^{-1}$  and the remanent polarization,  $P_r$ , is observed to be  $0.05 \mu\text{C cm}^{-2}$ . The finite remanent polarization can be attributed to the self-polarization behavior of

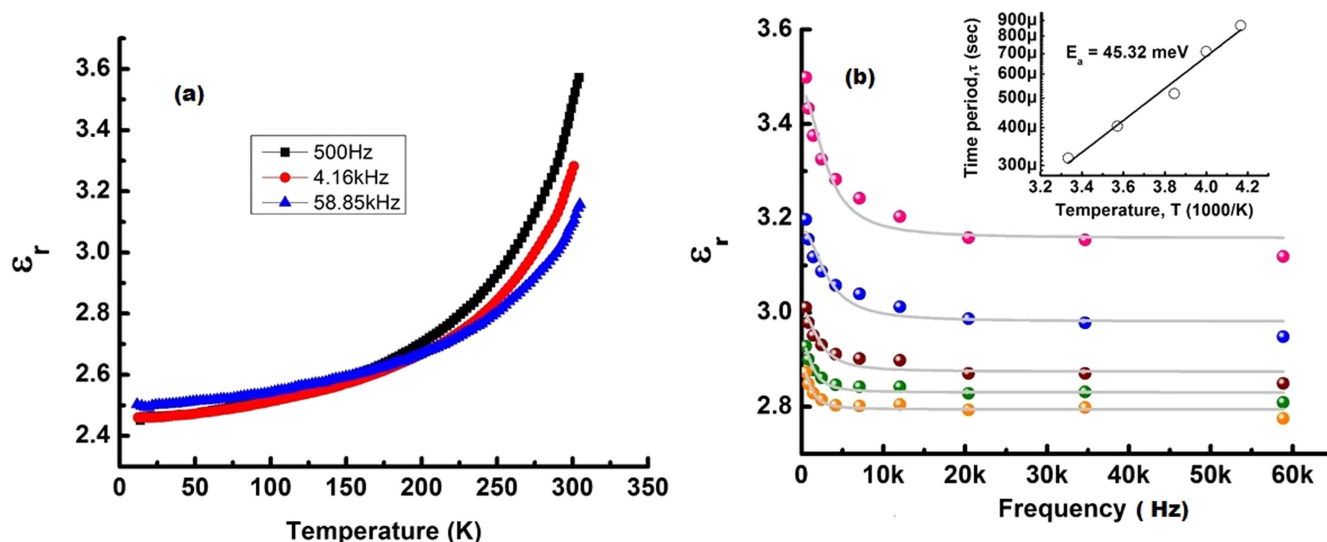


**Figure 3.** (a) The real part of a dielectric constant,  $\epsilon_r$ , versus the temperature plots of BSA-Au<sub>20</sub> at a frequency of 500 Hz, 4.16 kHz and 58.85 kHz, represented by black boxes, red circles and blue triangles respectively; (b)  $\epsilon_r$  versus the frequency plots of BSA-Au<sub>20</sub> at 300 K, 280 K, 260 K, 240 K and 220 K represented by pink, blue, magenta, green and yellow spheres respectively. The solid lines are the fitted curves. The inset is the relaxation time period versus the temperature plot obtained from the fitting. Using the Arrhenius-fitting, the activation energy is estimated to be 45.32 meV.

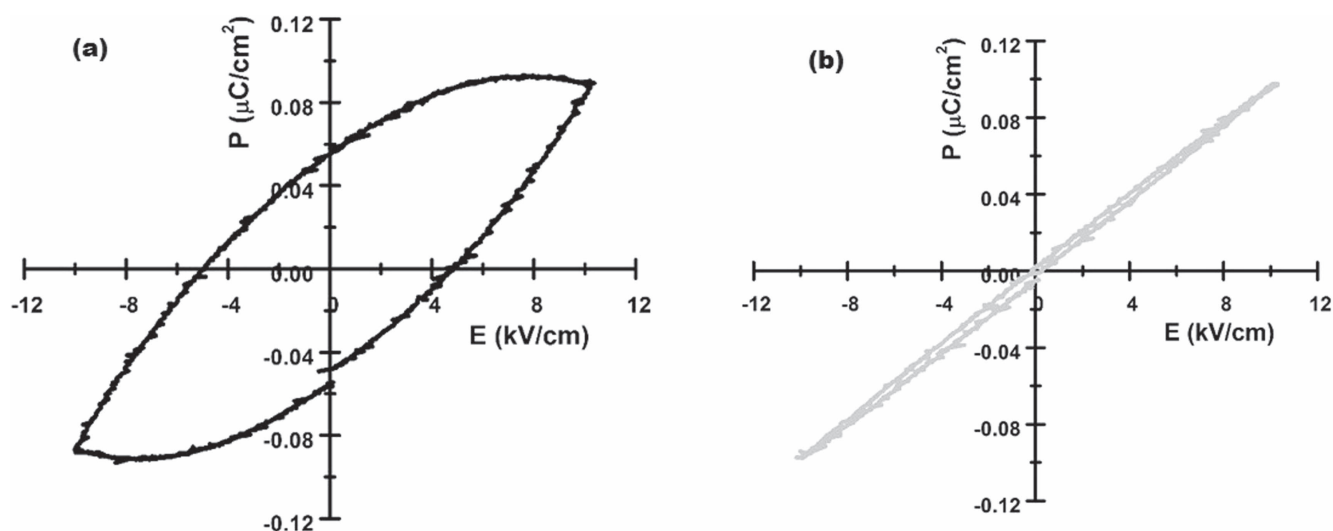


**Figure 4.** (a) The electric polarization (PE) loop of the BSA-Au<sub>20</sub>; (b) the PE loop of the BSA under the same condition. The PE studies have been carried out in the presence of a poling field  $4.5 \text{ kV cm}^{-1}$  at a frequency of 200 Hz and a temperature of 300 K.

the sample. A similar  $P_r$  ( $0.11 \mu\text{C cm}^{-2}$ ) has been observed by Chand *et al* from the zinc-oxide nanomaterial [29]. In our studies, the PE loop of the BSA shown in figure 4(b) exhibits a line-like loop passing through the origin, which indicates the predominantly para-electric character of the pure BSA.

To further understand the electronic polarization, we have optimized the Au<sub>20</sub> geometry using a B3LYP (Becke three parameter Lee–Yang–Parr) functional with LANL2DZ (Los Alamos National Laboratory 2-double Zeta) basis set for a singlet state in the platform based on density functional theory (DFT), utilizing the Gaussian-09 package. Figure 5(a) shows the optimized geometry of Au<sub>20</sub>. The electronic density of the highest occupied molecular orbital (HOMO) and the lowest unoccupied molecular orbital (LUMO) of the Au<sub>20</sub> were

calculated using the DFT-B3LYP/LANL2DZ theory level. As observed in figures 5(b) and (c), the calculated HOMO and LUMO electronic states exhibit a significant deformation in the charge density (the green and maroon color represent the positive and negative isosurface states respectively) and predict the existence of electronic polarization.

In summary, twenty gold atom clusters, synthesized using an aqueous-based growth technique, showed a spontaneous electric dipole moment. The emission properties of the sample corroborated the existence of the well-defined HOMO-LUMO gap (gap energy  $\sim 1.93 \text{ eV}$ ) with a strong dipolar oscillator strength. Temperature- and frequency-dependent dielectric studies confirmed the low dispersive dipolar orientation with an activation energy of  $\sim 45.32 \text{ meV}$ . The electric polarization

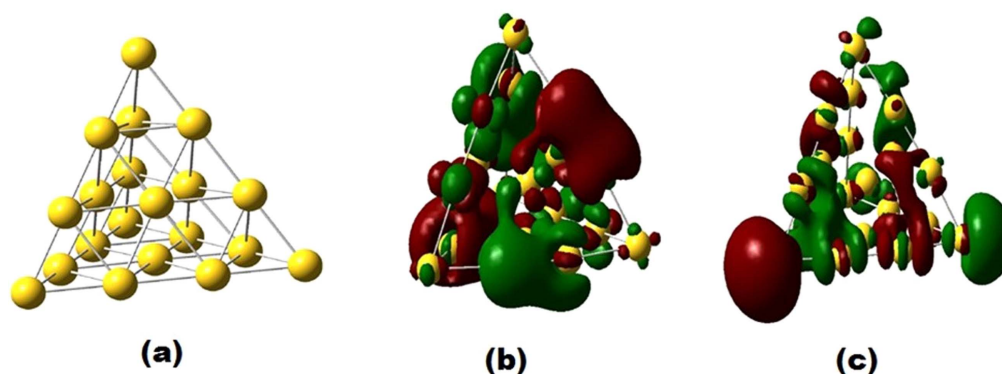


**Figure 5.** (a) The geometry-optimized structure of the Au<sub>20</sub> using Gaussian-09 software. A plot of the electronic charge density of (b) the highest occupied molecular orbitals and (c) the lowest unoccupied molecular orbitals of the Au<sub>20</sub> respectively. The green and maroon color represent the positive and negative states. The isovalue was taken to be 0.02 for the color plots.

properties at 300 K reveal a self-polarization effect with a remanent polarization of  $0.05 \mu\text{C cm}^{-2}$ . As observed from the DFT level calculation, the deformation of the charge density in the HOMO-LUMO states originated from the structural anisotropy yielding the spontaneous electric dipole moment. These results provide evidence that Au<sub>20</sub> gold clusters are a suitable material for self-powered electronic devices.

## Acknowledgments

The corresponding author (S R) acknowledges Dr B Satpati, Saha Institute of Nuclear Physics, 1/AF Bidhannagar, Kolkata-700 064, India, for the help received with the TEM measurements. S R also acknowledges Mr A Pradhani and Mr S Karmakar, IIT Bhubaneswar, for the assistance received during the experiments.

## ORCID iDs

A K Singh  <https://orcid.org/0000-0003-4401-2145>

## References

- [1] Ghosh S K and D Mandal D 2016 Self-powered flexible electronics based on self poled 'ferroelectric' nanogenerator *MRS Advance* **1** 3083–8
- [2] Pruvost S, Hajjaji A, Lebrun L, Guyomar D and Boughaleb Y 2010 Domain switching and energy harvesting capabilities in ferroelectric materials *J. Phys. Chem. C* **114** 20629–35
- [3] Hu W J, Juo D-M, You L, Wang J, Chen T-C, Chu Y-H and Wu T 2014 Universal ferroelectric switching dynamics of vinylidene fluoride-trifluoroethylene copolymer *Sci. Rep.* **4** 4772
- [4] Takasu H 2000 The ferroelectric memory and its application *J. Electroceramics* **4** 327–38
- [5] Rorvik P M, Grande T and Einarsrud M-N 2011 One-dimensional nanostructures of ferroelectric perovskites *Adv. Mater.* **23** 4007–34
- [6] Pradhani A, Halder O, Nozaki S and Rath S 2015 Raman modes, dipole moment and chirality in periodically positioned Au<sub>8</sub> clusters *RSC Advance* **5** 65208–13
- [7] Rath S, Nozaki S, Palagine D, Matulis V, Ivashkevich O and Maki S 2010 Aqueous-based synthesis of atomic gold clusters: geometry and optical properties *Appl. Phys. Lett.* **97** 053103
- [8] Andersen K E, Kumar V, Kawazoe Y and Pickett W E 2006 Origin and temperature dependence of the electric dipole moment in niobium clusters *Phys. Rev. B* **73** 125418
- [9] Ma L, Moro R, Bowlan J, Kirilyuk A and de Heer W A 2014 Multiferoic rhodium clusters *Phys. Rev. Lett.* **113** 157203
- [10] Wang J, Yang M, Jellinek J and Wang G 2006 Dipole polarizabilities of medium-sized gold clusters *Phys. Rev. A* **74** 023202
- [11] Moro R, Xu X, Yin S and de Heer W A 2003 Ferroelectricity in free niobium clusters *Science* **300** 1265–9
- [12] Andersen K E, Kumar V, Kawazoe Y and Pickett W E 2004 Origin of spontaneous electric dipoles in homonuclear niobium clusters *Phys. Rev. Lett.* **93** 246105
- [13] Link S, Beeby A, FitzGerald S, El-Sayed M A, Schaaff T G and Whetten R L 2002 Visible to infrared luminescence from a 28-atom gold cluster *J. Phys. Chem. B* **106** 3410–5
- [14] Li J, Li X, Zhai H-J and Wang L-S 2003 Au<sub>20</sub>: a tetrahedral cluster *Science* **299** 864–7
- [15] Wu K, Li J and Lin C 2004 Remarkable second-order optical nonlinearity of nano-sized Au<sub>20</sub> clusters: a TDDFT study *Chem. Phys. Lett.* **388** 353–7
- [16] Zhu M, Qian H and Jin R 2009 Thiolated-protected Au<sub>20</sub> clusters with a large energy gap of 2.1 eV *J. Am. Chem. Soc.* **131** 7220–1
- [17] Wan X K, Lin Z-W and Wang Q-M 2012 Au<sub>20</sub> nanocluster protected by hemilabile phosphines *J. Am. Chem. Soc.* **134** 14750–2
- [18] Henry C H and Nassau K 1970 Lifetimes of bound excitons in CdS *Phys. Rev.* **1** 1628–34
- [19] Wu Z and Jin R 2010 On the ligand's role in the fluorescence of gold nanocluster *Nano Lett.* **10** 2568–73
- [20] Raut S, Chib R, Rich R, Shumilov D, Gryczynski and Gryczynski I 2013 Polarization properties of fluorescent BSA protected Au<sub>25</sub> nanoclusters *Nanoscale* **5** 3441–6
- [21] Tian X, Wu Z, Jia Y, Chen J, Zheng R K, Xhang Y and Luo J 2013 Remanent-polarization-induced enhancement of photoluminescence in Pr<sup>3+</sup>-doped lead-free ferroelectric (Bi<sub>0.5</sub>Na<sub>0.5</sub>)TiO<sub>3</sub> ceramic *Appl. Phys. Lett.* **102** 042907
- [22] Wan X-K, Yuan S-F, Lin Z-W and Wang Q-M 2014 A chiral gold nanocluster Au<sub>20</sub> protected by tetradentate phosphine ligands *Angew. Chem. Int. Ed.* **53** 2923–6
- [23] Knoppe S, Zhang Q-F, Wan X-K, Wang Q-M, Wang L-S and Verbiest T 2016 Second-order nonlinear optical scattering

- properties of phosphine protected Au<sub>20</sub> clusters *Ind. Eng. Chem. Res.* **55** 10500–6
- [24] Murali P 2000 Ferroelectric thin films for micro-sensors and actuators: A review *J. Micromech. Microeng.* **10** 136–46
- [25] Dutta K and De S K 2007 Double dielectric relaxation in SnO<sub>2</sub> nanoparticles dispersed in conducting polymer *J. Appl. Phys.* **102** 084110
- [26] Wang X, Chen K-P, Zhao M and Nolte D D 2010 Refractive index and dielectric constant evolution of ultra-thin gold from clusters to films *Opt. Express* **18** 24859–67
- [27] Abdelhalim M A K, Mady M M and Ghannam M M 2011 Dielectric constant, electrical conductivity and relaxation time measurements of different gold nanoparticle sizes *Int. J. Phys. Sci.* **6** 5487–91
- [28] Badr A M, Elshaikh H A and Ashraf I M 2011 Impact of temperature and frequency on the dielectric properties for insight into the nature of the charge transports in Tl<sub>2</sub>S layered single crystals *J. Mod. Phys.* **2** 12–25
- [29] Chand P, Gaur A and Kumar A 2013 Study of optical and ferroelectric behavior of ZnO nanostructure *Adv. Mat. Lett.* **4** 220–4